MICROBIAL ECOLOGY

Microb Ecol (1999) 37:185–196
DOI: 10.1007/s002489900142

Linking Sediment Biofilms, Hydrodynamics, and River Bed Clogging: Evidence from a Large River

T.J. Battin,[1] D. Sengschmitt[2]

[1] Department of Ecology, University of Vienna, Althanstrasse 14, A-1090 Vienna, Austria
[2] Institute of Hydraulics, Hydrology and Water Resources Management, Vienna University of Technology, Karlsplatz 13, A-1040 Vienna, Austria

Received: 14 September 1998; Accepted: 31 December 1998

Abstract

We investigated possible effects of the hydrodynamics at the water/sediment interface on river bed biofilms within the reservoir Freudenau (Vienna, Austria) of the Danube River during the period 1996/97. Two study sites (OBB and SSF) that differed in the magnitude of surface/subsurface water exchange were selected and intersite comparisons revealed higher organic matter, bacterial cell numbers, and esterase activity in SSF with lower horizontal outflow. Concentrations of colloidal carbohydrates and uronic acids were unaffected by hydrodynamics. The relative contribution of uronic acids to bulk colloidal carbohydrates was higher in the low-flow site SSF. The distribution patterns of this relative contribution generally matched the subsurface flow pattern. Shortly after impoundment in March 1996 and along with decreased surface flow velocity, maximal biofilm carbohydrate exopolymers concurred with minimal esterase activity in OBB. We hypothesize that this inverse relationship is due to increased diffusional resistance within the exopolymer biofilm matrix that reduces mass transfer and hydrolytic activity.

These results, to our knowledge, are the first evidence for microbial participation in the clogging of a large river bed. Biofilm-associated organic carbon increased significantly by a factor of ~3.3 to 4.4 with progressive clogging as determined by the sediment leakage coefficient, which increased ~3.8 times. Concomitantly, with ongoing clogging, esterase activity exhibited increasingly higher values at the interface relatively to deeper sediment layers, which translates into steeper depth gradients. Furthermore, minimal inflow from the surface water into the river bed along with steepest esterase gradients concurred with a senescent benthic algal bloom. This suggests an important role for algae in clogging. Either algae obstruct voids mechanically, or their exudates fuel heterotrophic bacteria that in turn are involved in clogging processes. However, our data do not allow unequivocal differentiation between biogenic and physical clogging mechanisms.

Correspondence to: T.J. Battin; Fax: # 1 31336 776; E-mail: tomba@pflaphy.pph.univie.ac.at

Introduction

Biofilm bacteria predominate both numerically and metabolically in lotic systems, where they largely determine fluxes of nutrients, energy, and matter (e.g., [26]). Heterotrophic bacteria assimilate dissolved organic carbon and concomitantly synthesize substantial amounts of carbon in the form of capsular and extracellular polysaccharides [10, 37]. Extracellular production is stimulated by cell attachment [43] and its accumulation results in the biofilm matrix. The functions of the matrix are multiple [22, 26]: in addition to mediation of adherence to surfaces, they range from protection against stress, e.g., through alleviated nutrient and carbon supply [17], to the transfer of exopolysaccharides to higher trophic levels [10].

Hydrodynamics is a chief factor that drives the functioning of microbial biofilms on several levels. Whereas diffusion is likely the major mass transfer vector in homogeneous biofilms, convective transport of solutes becomes increasingly important in heterogeneous biofilms [9, 36]. On a higher scale, hydrodynamics can shape stream biofilm architecture [3] by eroding and sloughing entire exopolymer fragments and cellular aggregates. Furthermore, the mass transfer from the surface water to the sediment and hence to biofilms depends on hydrodynamics along with bed morphology (e.g., [12]). Ultimately, hydrodynamics constrains erosion and sedimentation zones and accumulation of particles and bed material (e.g., [4]).

There is emerging evidence that microorganisms also affect hydrodynamic processes in porous media such as river bed sediments. The accumulation of biofilm exopolymers [41], and also bacterial cells [42] and their gaseous metabolites [27], can reduce the hydraulic conductivity of saturated soils and aquifer material. Clogging of porous media becomes particularly important to the operation of production and injection wells. Microbial exopolysaccharides also stabilize cohesive sediment and reduce erosion in coastal marine systems (e.g., [18]).

Despite their potential relevance on multiple ecological scales, microbial biofilms have long been neglected in streams and particularly in rivers [24]. The lack of appropriate techniques enabling field studies and laboratory models have largely hampered research on lotic biofilms. Those studies attempting to integrate microbial ecology and hydrodynamics are either related to headwater streams or have been rather qualitative (e.g., [5, 19]).

The present article represents the first comprehensive endeavor to describe natural sediment biofilms from a large river and to quantitatively relate them to surface/subsurface water exchange processes. Vessel-based freeze-coring allowed us to collect sediment cores and to sample biofilms to a depth of 90 cm. Our objectives were twofold: (i) to relate the effect of hydrodynamics on the spatial and temporal variation of biofilms, with particular emphasis on carbohydrate exopolymers and esterase activity; and (ii) to explore possible participation in microbial biofilms in the clogging of the Danube River bed caused by hydropower impoundment.

Study Site

Sediment cores were taken in the Danube River at "Ostbahnbrücke" (OBB, river-km 1925.1) and "Schulschiff" (SSF, river-km 1931.4) within the reservoir Freudenau (hydropower dam at river-km 1921.1), Vienna, Austria. Within this reach, the Danube River (9th order) has an average channel width of 270 m and a bed slope of 0.4‰. River flow is regulated and discharge ranged from 770 to 6700 $m^3\ s^{-1}$ (average 1700 $m^3\ s^{-1}$) during the study period 1996/97 (Fig. 1). Impounding in March 1996 increased the water level by ~6 m at the dam, which caused a water level increase of ~3 and ~5.5 m in SSF and OBB, respectively. Concomitantly, flow velocity declined from a preimpounding average of 1.6 m s^{-1} to 1.0 and 0.7 m s^{-1} in SSF and OBB, respectively. Decreased flow velocity along with permanent surface water inflow into the river bed caused increasing sedimentation rates and thereby substantial clogging at the water/sediment interface.

Hydrogeologic Setting

We computed subsurface maximum horizontal outflow through the left bank of the Danube River from a water balance of fringing reservoirs, the right bank having a man-made impervious wall. Piezometric measurements in the river bed (SSF) and at the left bank (SSF and OBB) and a one-dimensional analytical steady state profile model [29] were used to compute the leakage coefficient of the clogged sediment layer and both the vertical inflow and horizontal outflow velocities [33]. The leakage coefficient (see Fig. 1), which is the ratio between the hydraulic conductivity and the sediment thickness affected, describes the degree of clogging. The temporal variation of the leakage coefficient as determined in SSF is shown in Fig. 1. In OBB, a similar temporal pattern could be estimated from piezometric data.

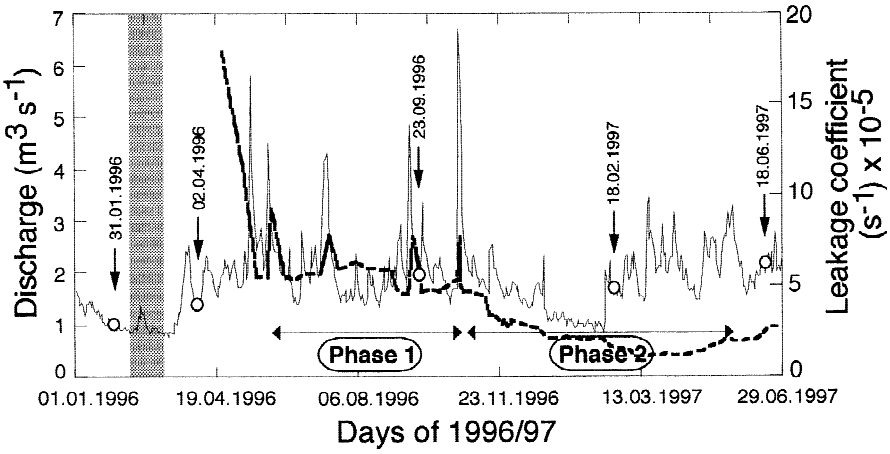

Fig. 1. Discharge of the Danube River and leakage coefficient (bold line) of the river bed at site SSF for 1996/97. The shaded bar denotes the beginning of impoundment; arrows refer to the sampling dates. Phases 1 and 2 designate progressive clogging.

The thickness of the clogged layer was theoretically less than 0.5 m as derived from piezometric data. This was confirmed by scuba divers who visually estimated a thickness of 0.05–0.2 m from in situ sediment profiles. The thickness of the aquifer (Table 1) was estimated from deep cores that were retrieved along both banks of the Danube River. The aquifer consists of quaternary sandy gravel and is underlain by an impermeable layer of silt and clay. Knowing their respective thickness, the hydraulic conductivity could now be determined for the clogged layer and the aquifer. The hydraulic conductivity (m s^{-1}) is a descriptor of the water flux through a permeable porous medium along a hydraulic gradient of 1.

Analyses of grain size distributions [35] revealed fairly low spatial variability of the hydraulic conductivity that ranged from 8×10^{-3} to 8×10^{-4} m s^{-1}. During the preimpounding period, the hydraulic conductivity did not differ between surface and aquifer sediments in both SSF and OBB. According to the piezometric data, the aquifer hydraulic conductivity averaged 6×10^{-3} m s^{-1} in SSF. As a consequence of impounding, the surface sediment hydraulic conductivity decreased by ca. 2 to 3 orders of magnitude within the first 3 months to further decline by a factor of 10, which translates into a five- to sixfold decrease of the leakage coefficient. This partitioned the clogging process into two major phases (Fig. 1) that are relevant to the present study.

This configuration generated a clearly segregated flow pattern (Fig. 2) that is described in detail by Sengschmitt et al. [33]. Briefly, vertical inflow of surface water occurred through the clogged sediment, whereas horizontal outflow occurred through deeper regions towards the groundwater adjacent to the left bank. The maximum horizontal outflow was approximately 4–5 times higher in OBB than SSF (see Table 1, Fig. 2). By contrast, vertical inflow velocities were consistently lower in both SSF (~6 times, corresponding to maximal 0.08×10^{-4} m s^{-1}) and OBB (~16 times, corresponding to maximal 0.13 to 0.19×10^{-4} m s^{-1}) than the horizontal flow velocity. This resulted in similar average vertical inflow velocities in OBB and SSF sampling sites. These were located approximately 60–90 m in SSF and 50–120 m in OBB from the left bank where horizontal outflow velocities accounted for 20–40% (Fig. 2A) of their maximal values.

Methods

Sampling and Preanalytical Sample Handling

Sediment cores (90 cm) were collected with a vessel-based freeze core technique as modified for large and deep rivers by Humpesch and Niederreiter [20] and designed by UWITEC, Austria. Shock-frozen (liquid N_2) sediment cores were partitioned into 10 cm depth layers on the vessel and aliquots were stored frozen (−20°C)

Table 1. Hydrogeologic setting of the Danube River study sites SSF and OBB

Study site	Hydraulic conductivity (m s^{-1})		Sediment thickness (m)		Maximal outflow velocity at the left bank (m s^{-1})
	Clogged layer	Aquifer	Clogged layer	Aquifer	
SSF	10^{-5}–10^{-6}	6×10^{-3}	0.05–0.20	5	0.5×10^{-4}
OBB	10^{-5}–10^{-6}	~5×10^{-3}	0.05–0.20	2.5	2.0–3.0×10^{-4}

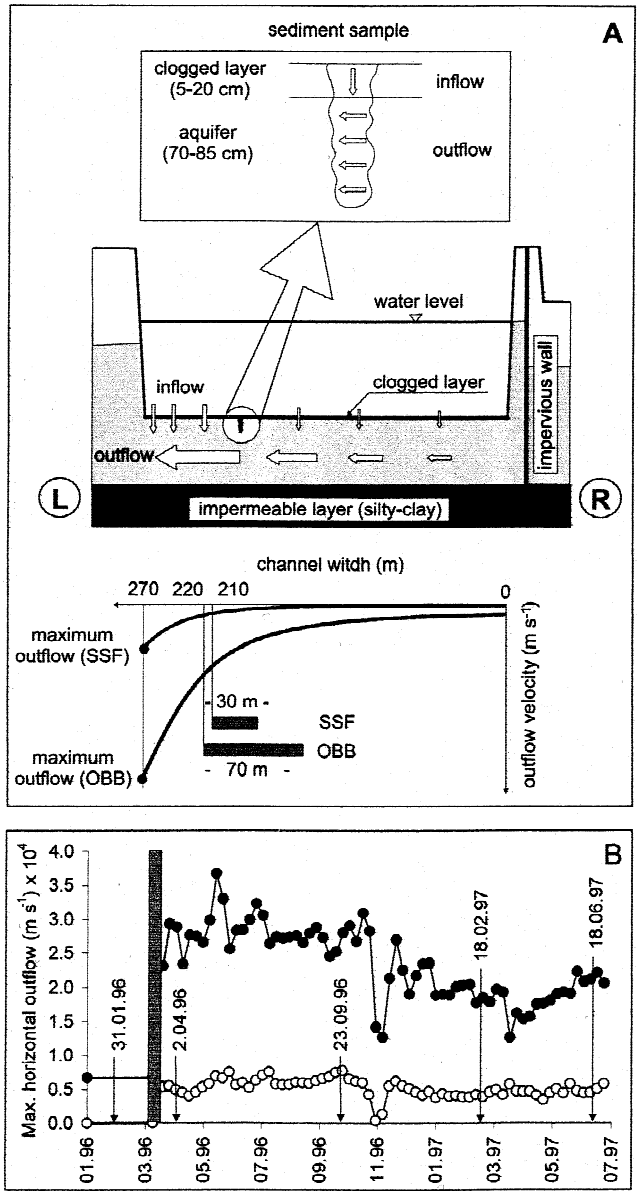

Fig. 2. (A) Representative transect through the Danube River within the Freudenau reservoir; R and L designate orographic right and left banks. The upper inset shows the location of a sediment core in relation to the flow patterns as described in the text. The lower inset illustrates the spatial variability of the outflow across the transect. Shaded bars represent the sampling areas in OBB and SSF. (B) Temporal variation of maximum horizontal outflow velocity in OBB (closed dots) and SSF (open dots). Arrows in the bottom frame designate the sample dates; the shaded bar designates the beginning of impoundment.

pending laboratory analyses. Two to three replicate cores were retrieved per date in SSF and OBB. Prior to analyses, samples were thawed and gently sieved to retain the grain size fraction 63–1000 μm, which contains the bulk organic matter [25]. Thawed sediment was immediately processed as described below.

Carbohydrate Exopolymers

Carbohydrate exopolymers were extracted with 50 mM EDTA from ca. 5 g (dry mass) sediment on a rotating shaker for 1 h (20°C). Samples were subsequently centrifuged and filtered (Whatman GF/F) to remove particles. Carbohydrates in the supernatant are referred to as colloidal (C–CHO) [40] and, according to Underwood et al. [40], are thought to include components that are closely associated with sediment and bacterial capsules. Bulk C–CHOs were hydrolyzed in sulfuric acid (100°C, 30 min) and assayed according to Dubois et al. [11]. Uronic acid (UAc) concentrations were measured in the same supernatant by the modified *m*-hydroxydiphenyl (MHDP) method by Filisetti-Cozzi and Carpita [14], which prevents interference with neutral sugars. UAcs were hydrolyzed with a 75 mM sodium tetraborate solution in sulfuric acid (100°C, 30 min). Both assays were run in duplicate and calibration was via a standard curve of absorbance versus glucose (485 nm) and glucuronic acid (525 nm) for C–CHOs and UAcs, respectively. Absorbance was measured with a Zeiss UV-VIS spectrophotometer. Since the phenol–sulfuric acid method for C–CHO also targets UAcs, both fractions were converted into carbon equivalents to calculate the relative UAc contribution to the C–CHO pool.

Bacterial Abundance

Bacterial abundance was estimated by epifluorescence microscopy after staining with 4′,6-diamidino-2-phenylindole (DAPI, Sigma, St. Louis, MO) according to Porter and Feig [32]. Approximately 1–2 g (wet mass) sediment preserved in formaldehyde (2.5%) was incubated with 0.1 M tetrasodium pyrophosphate for 30 min and subsequently sonicated for 3 × 60 s at a ~50 W output to detach bacterial cells from sediment surfaces [44]. The supernatant was diluted as appropriate with 0.2 μm filtered Milli-Q water. One milliliter of this suspension was stained with 50 μl DAPI (100 μg ml^{-1}). After 15 min the sample was filtered (<200 mbar vacuum) through a black 0.2 μm GTBP Millipore filter that was mounted onto a 0.2 μm filter (GSWP Millipore) to achieve even cell and particle distribution. The filter was washed (0.2 μm filtered Milli-Q water) and mounted in nonfluorescent immersion oil on a microscopic slide. Bacterial cells were enumerated in 10–30 randomly selected fields to account for at least 300 cells.

Esterase Activity

Esterase activity was assayed with fluorescein diacetate (FDA, Sigma, St. Louis, USA) according to Battin [1] except that we suspended the sediment (2–3 g wet mass) in phosphate buffer (pH = 7.6) [16] instead of filtered river water. Triplicate trials were incubated at a final concentration of 200 μM FDA. After a 30 min incubation period, the hydrolysis was stopped with acetone and the samples were put on ice. Fluorescein was extracted by sonicating (45 s, 30 W output) the suspension, and particles were removed by centrifugation (8°C, 20 min, 5000 rpm). The absorbance of the supernatant was measured at 490 nm and Na_2-fluorescein (Serva, p.a. grade) was used as standard. Duplicate blanks were inactivated

with 50% (vol/vol) acetone for 30 min prior to the addition of the FDA solution. Previous experiments revealed no significant effect of liquid nitrogen shock freezing on sediment biofilm esterase activity.

Chlorophyll a

Chlorophyll *a* was extracted with analytical grade acetone from 2–3 g (wet mass) sediment in the dark (4°C) for 12 h followed by centrifugation. The absorbance of the supernatant was measured with a Hitachi U-2000 spectrophotometer. For pheophytin analysis, 2 drops of 10% HCl were added and the absorbance was measured again. Concentrations of chlorophyll *a* and pheophytin were estimated according to Parsons et al. [31].

Total Organic Matter

The total organic matter of the sediment was estimated by ignition loss on ca. 10 g dry mass sediment (550°C, 4 h). We assumed that 50% of the total organic matter was organic carbon (e.g., [45]).

Statistical Analyses

Comparisons between sites and among dates were accomplished with analyses of variance (ANOVA) and the Tukey test for multiple comparison on log(x+1) transformed data. The relationship between C–CHO and UAc concentrations was analyzed with least square regressions and slopes were compared with the Student's t-test [16]. The variation of biofilm esterase activity was explored with stepwise multiple regression analysis. Step order was forward, p to enter was 0.15, and minimum tolerance for entry into the model was 0.01. If necessary, adjacent depth layers were pooled in order to increase the degrees of freedom. All tests were considered significant at the level $\alpha = 0.5$ and values are given as mean ± standard error (S.E.). Analyses were performed with SYSTAT [46]. All biofilm parameters are expressed per gram dry mass (DM) of sediment.

Results

Effects of Hydrodynamics on Biofilms

SSF sediment exhibited apparently higher average biomass and esterase activity than OBB sediment (Fig. 3). Site effects were most pronounced on TOC ($F = 103.68$, $p < 0.0001$, $n = 166$) with average values of 6.46 ± 0.42 and 1.28 ± 0.07 mg C g^{-1} DM in SSF and OBB, respectively. Bacterial abundance ($F = 19.874$, $p < 0.0001$, $n = 63$) and biofilm esterase activity ($F = 4.986$, $p = 0.027$, $n = 182$) also differed significantly between sites with respective average values of 21.09 ± 3.44 × 10^9 cells g^{-1} DM and 7.99 ± 1.00 μmol FDA g^{-1} DM h^{-1} in SSF and 3.13 ± 0.79 × 10^9 cells g^{-1} DM and 13.54 ± 1.49 μmol FDA g^{-1} DM h^{-1} in OBB. Although most parameters declined toward depth, significant changes were only detected in SSF esterase activity (ANOVA, $F = 9.210$, $p < 0.0001$; Tukey's test 0–10 cm: $p < 0.001$; 10–20 cm: $p < 0.001$).

No significant site effect was found on carbohydrate exopolymers (Fig. 3). C–CHO concentrations averaged 4.97 ± 0.72 and 4.77 ± 0.33 μg C g^{-1} DM in SSF and OBB, respectively, and UAc concentrations averaged 3.61 ± 0.62 and 2.41 ± 0.17 μg C g^{-1} DM in SSF and OBB, respectively. Nor were we able to directly relate sugar concentrations in the shallow sediment to inflow velocities (C–CHO: $r = 0.058$, $p = 0.881$; UAc: $r = 0.076$, $p = 0.845$). However, decreasing depth gradients of relative UAc contribution to bulk C–CHOs were apparent in SSF (Table 2). We explored the UAc contribution by comparing the slopes of linear regressions with C–CHOs entering the model as independent and UAc concentration as dependent variable. The SSF 0–20 cm slope was significantly ($t = 4.222$, $p < 0.01$) higher than the 60–90 cm slope, which translates into C–CHO:UAc ratios of ca. 1.71 and 2.86 in shallow and deep layers, respectively.

The most salient temporal pattern is the disparity between carbohydrate concentrations and esterase activity shortly after the impoundment (Fig. 4). In OBB, C–CHO and UAc concentrations increased significantly from 6.58 ± 0.39 to 13.51 ± 1.65 μg C g^{-1} DM and from 3.26 ± 0.32 to 8.55 ± 1.43 μg C g^{-1} DM, respectively, to subsequently return to preimpounding levels. This peak concurred with minimal esterase activity (0–10 cm: 2.24 ± 2.37 μmol FDA g^{-1} DM h^{-1}) that gradually increased after the impoundment. Lowest bacterial cell numbers coincided with minimal esterase activity; their temporal variation, however, was not significant.

Microbial Biofilms and River Bed Clogging

In order to test possible microbial participation in the clogging process of the river bed, we first explored impounding effects of the biofilm associated organic carbon. Knowing the concentration of C–CHO carbon, assuming 20 fg C per bacterial cell [25] and a carbon to chlorophyll *a* ratio of 25 (e.g., [6]) we estimated the average biofilm carbon in the shallow (0–20 cm) sediment layer that is affected by clogging. At both sites, we found significantly higher organic carbon concentrations in the shallow sediment layer during the second clogging phase (Fig. 5). Carbon concentrations increased by a factor of ~3.3 and ~4.4 in SSF and OBB, respectively, from the first to the second clogging phase. The leakage factor decreased by a factor of ~3.8 from 5.4 to 1.4 × 10^{-5} s^{-1} from

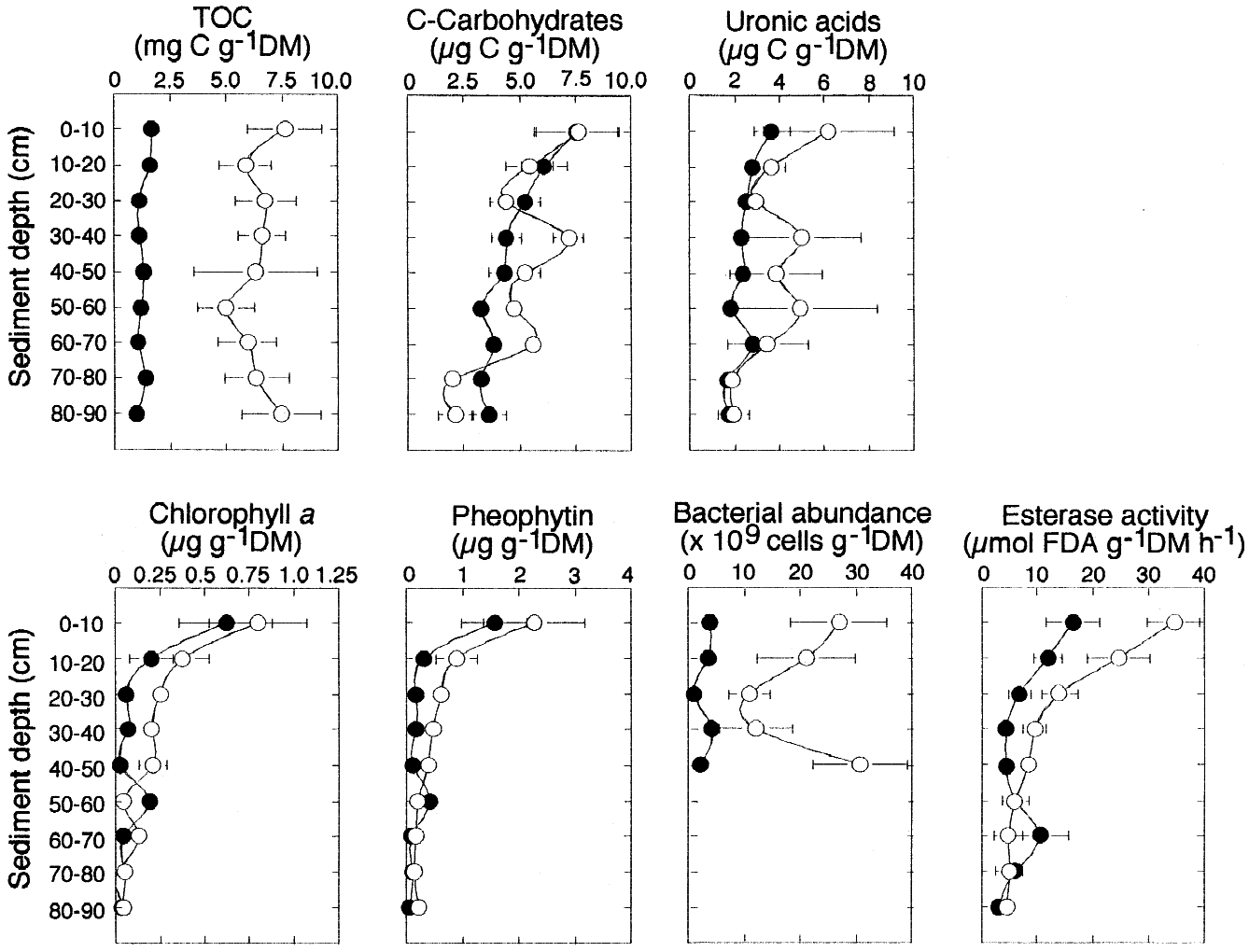

Fig. 3. Depth gradients of biofilm parameters analyzed in sediment cores from the Danube River bed. Closed dots refer to the OBB and open dots to the SSF channel site. Dots indicate mean (temporal and spatial) values ±S.E.

the first to the second clogging phase. No significant increases, however, could be detected between the preimpounding period and clogging phase 1.

Second, we hypothesize that depth gradients of esterase activity become steeper with ongoing clogging and hence with decreasing vertical flow velocity. Depth gradients of esterase activity were operationally defined as the slope of the exponential model (see Fig. 6) that describes the hydrolytic rates (dependent variable) along depth (independent variable). In fact, we found hydrolytic gradients positively related ($r^2 = 0.62$, $p = 0.021$) to the vertical inflow velocity (Fig. 6).

Relationships among Biofilm Parameters

We used regression techniques to explore relationships among microbial biomass, esterase activity, and exopolymer carbohydrates in river bed biofilms. These variables showed, in fact, considerable covariation (Table 3) in the shallow SSF sediment, but not in OBB, where the average algal biomass (0–40 cm) was ~27% lower. As revealed by multiple regressions, chlorophyll *a* and pheophytin explained 77% ($F = 18.608$, $p < 0.001$) and 62% ($F = 9.051$, $p = 0.004$) of the variance in C–CHO and UAc concentration, respectively. Multiple regression showed that algal pigments along with bacterial cell numbers explained 83% ($F = 8.241$, $p = 0.022$) and 94% ($F = 25.46$, $p = 0.002$) of the variance in SSF mid-layer C–CHO and UAc concentration, respectively.

Although no direct relationship was apparent between bacterial abundance and algal biomass, stepwise multiple regression (Table 4) entered bacterial abundance as third independent variable to explain 52% of the variance in SSF esterase activity along with chlorophyll *a* and C–CHO con-

Table 2. Regression parameters of the relationship between C–CHO and UAc concentrations and C–CHO:UAc ratios along different river bed depths in the Danube River sites SSF and OBB

	Linear regression analysis						
Depth	Slope	S.E.	r^2	F	p	n	C–CHO:UAc ratio
Site SSF							
0–20 cm	0.670	0.050	0.88	179.5	0.0001	26	1.71 ± 0.09
20–40 cm	0.633	0.065	0.82	94.42	0.0001	23	1.94 ± 0.25
40–60 cm	0.582	0.048	0.89	146.4	0.0001	20	2.17 ± 0.23
60–90 cm	0.386	0.045	0.76	73.01	0.0001	25	2.86 ± 0.32
Site OBB							
0–20 cm	0.416	0.038	0.87	116.24	0.0001	19	2.19 ± 0.13
20–40 cm	0.409	0.067	0.69	37.556	0.0001	19	2.36 ± 0.20
40–60 cm	0.584	0.073	0.78	63.854	0.0001	20	2.06 ± 0.74
60–90 cm	0.489	0.149	0.43	10.693	0.0056	16	2.33 ± 0.19

centration. By contrast, in OBB where bacterial abundance was significantly lower, chlorophyll *a* and C–CHO concentrations explained 78% of the variance in biofilm esterase activity.

Discussion

Our results emphasize the interplay between hydrologic exchange and microbial biofilms at the surface/subsurface water interface of a large river bed. The direction and velocity of water flow through the river bed shaped microbial biomass and esterase activity and, as first evidence suggests, biofilms were related to the clogging of the river bed and thereby influenced hydrodynamics.

Hydrologic Control on Biofilms

We found low TOC, bacterial cell numbers, and esterase activity associated with elevated inflow velocities from the surface water into the river bed in OBB. Conversely, lower inflow velocities in SSF caused accumulation of biomass and esterase activity. Results from our intersite comparison thus agree with those of Claret and Fontvieille [5], who, investigating sediment biofilms from the Rhône River banks and adjacent sources, found higher TOC and bacterial numbers associated with low flow in sources. Yet they were not able to unequivocally partition the effect of hydrodynamics and grain size distribution. Similar grain size distributions in OBB and SSF (see Table 5) allowed us to exclude differing surface availability to colonization possibly blurring the intersite comparison. Average OBB and SSF TOC concentrations are closely bracketed by values reported from Danube [25] and Rhône sediments [28]. Our estimates of bacterial abundances, however, clearly outnumber Rhône sediment biofilms [28] but largely agree with estimates from Danube floodplain sediments [13].

On the other hand, flow velocity did not affect C–CHO and UAc concentrations. However, we found a prominent depth gradient of the relative UAc contribution to C–CHOs in SSF. We propose that increased sedimentation of particles clogs the shallow interstitial voids and subsequently inhibits mass transfer to the biofilm surface. The negative charge of UAcs that is conferred by the tertiary carboxyl group [7] renders UAcs particularly important in binding positively charged particles, colloids and metals (e.g., [2, 21]) to biofilms. Neu and Lawrence [30] have, in fact, confirmed considerable presence of detrital material in biofilms cultivated in rotating annular reactors from water of the South Saskatchewan River. Progressive sorption to the biofilm can increase the diffusional resistance within the matrix and subsequently reduce the solute flux to bacteria. This can induce physiological stress, which in turn has been reported to stimulate UAc synthesis [40] in bacteria. This hypothetical scenario is in fact supported by the match between subsurface flow (Fig. 2A) and C–CHO:UAc ratios. Horizontal outflow was consistently higher (ca. 6 times) than the vertical inflow and likely prevented particle accumulation in deeper SSF layers. Strikingly, deep river bed C–CHO:UAc ratios did not differ between both sites despite higher outflow velocities in OBB. Also, there were obvious intersite differences between the shallow river bed C–CHO:UAc ratios. The corresponding inflow values, however, varied only by an average factor of 2. This indicates that additional factors such as biomass, which was significantly higher in SSF (see Fig. 3), also influence the relative occurrence of sugars.

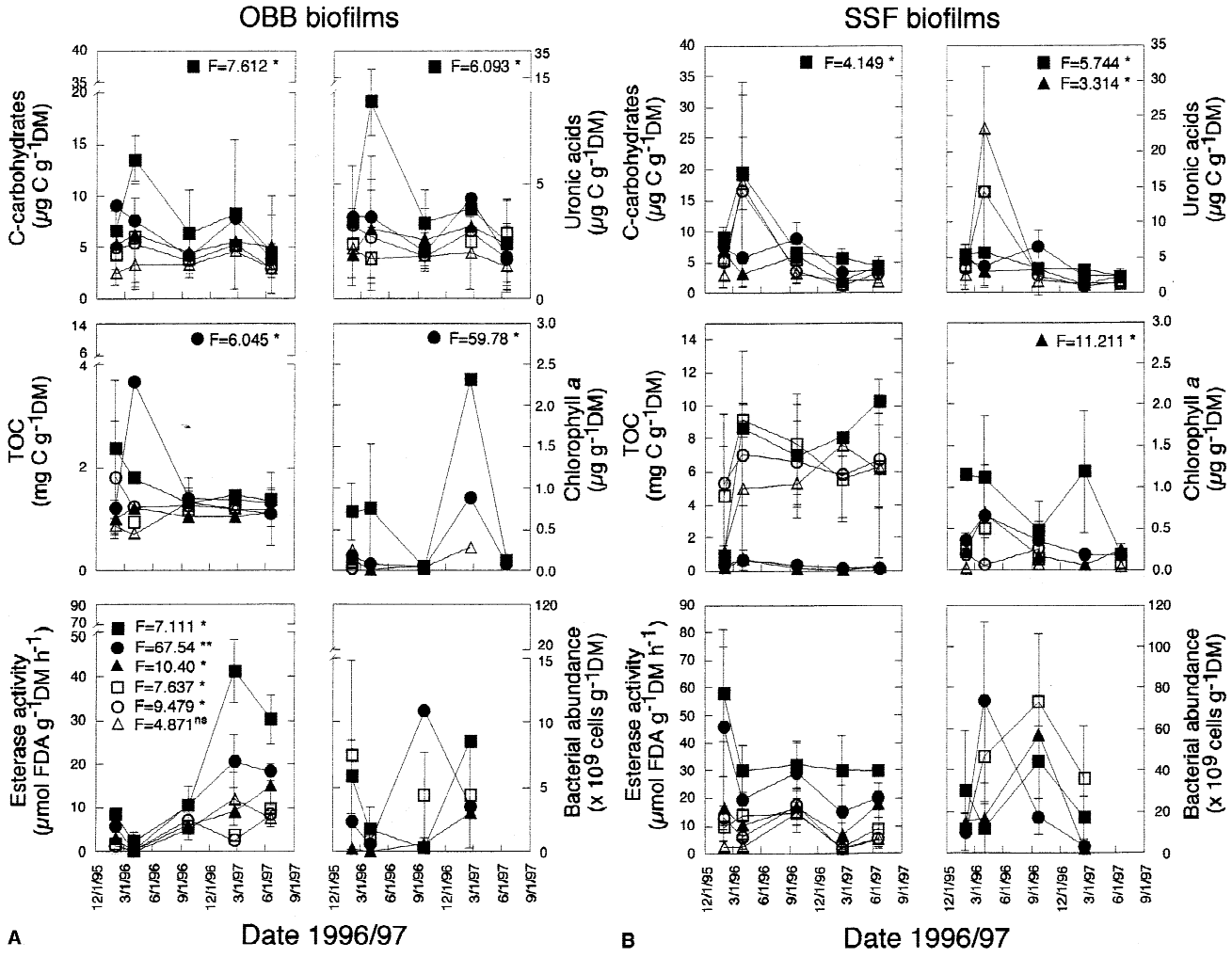

Fig. 4. Temporal patterns of selected biofilm parameters in Danube sediment cores (0–60 cm) from (A) OBB and (B) SSF. ANOVA on $\log(x + 1)$ transformed data tested for significant time effects (* is $p < 0.05$, ** is $p < 0.01$). Symbols are closed square: 0–10 cm, closed circle: 10–20 cm, closed triangle: 20–30 cm, open square: 30–40 cm, open circle: 40–50 cm, open triangle: 50–60 cm. Given are averages ±S.E. (spatial variation).

Similarly, the pronounced increase of biofilm exopolymers we observed shortly after impoundment might have been caused by the elevated particle sedimentation. The inverse relationship between biofilm CHOs and esterase activity is likely attributable to increased matrix thickness—which we measured as CHOs—which in turn increases the diffusional resistance to the mass transfer. Biofilm rate processes such as the hydrolysis of organic molecules (e.g., ester bonds) immobilized from the bulk liquid may thus become inhibited. We can exclude river discharge as a possible cause for the disparity between biomass and activity. In fact, the hydrologic situation prior to sampling (see Fig. 1) in March/April 1996 and February/March 1997 was similar with prolonged low discharge averaging 870 and 1000 $m^3\ s^{-1}$ in 1996 and 1997, respectively, and followed by floods. Biofilm patterns, however, differed between both sampling dates.

Linking Microbial Biofilms to River Bed Clogging

Our results are the first to link field data of biofilm accumulation and sediment clogging in a large river. We found an average increase of the biofilm-associated carbon of ~3.3 and ~4.4 in SSF and OBB, respectively, from the first to the second clogging phase. The leakage coefficient decreased by a factor of ~3.8 from 5.4 to $1.4 \times 10^{-5}\ s^{-1}$ during the same period. These relationships are largely consistent with research on model systems (e.g., [9, 33, 38, 42]) that related reduced hydraulic conductivity in sediment columns to in-

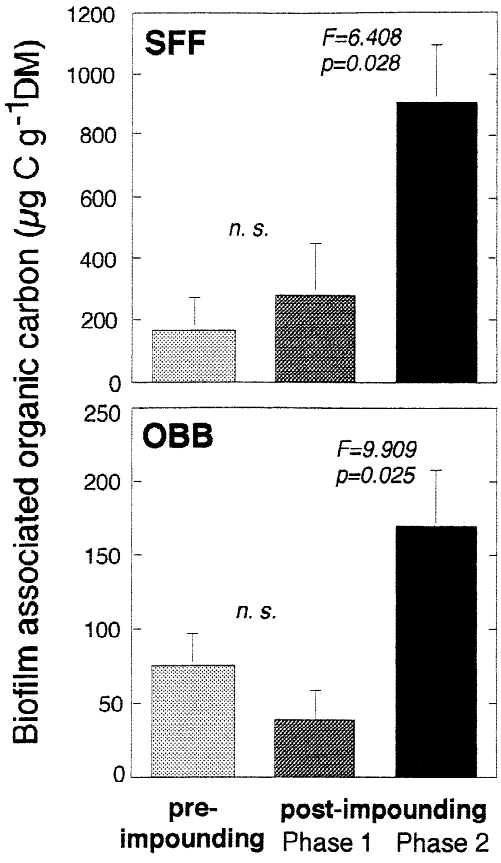

Fig. 5. Average (±S.E.) organic carbon concentrations associated with microbial biofilms during the pre- and post impounding period in the clogged layer (0–20 cm) of the Danube River bed. Phase 1 and 2 refer to the clogging process (see Fig. 1).

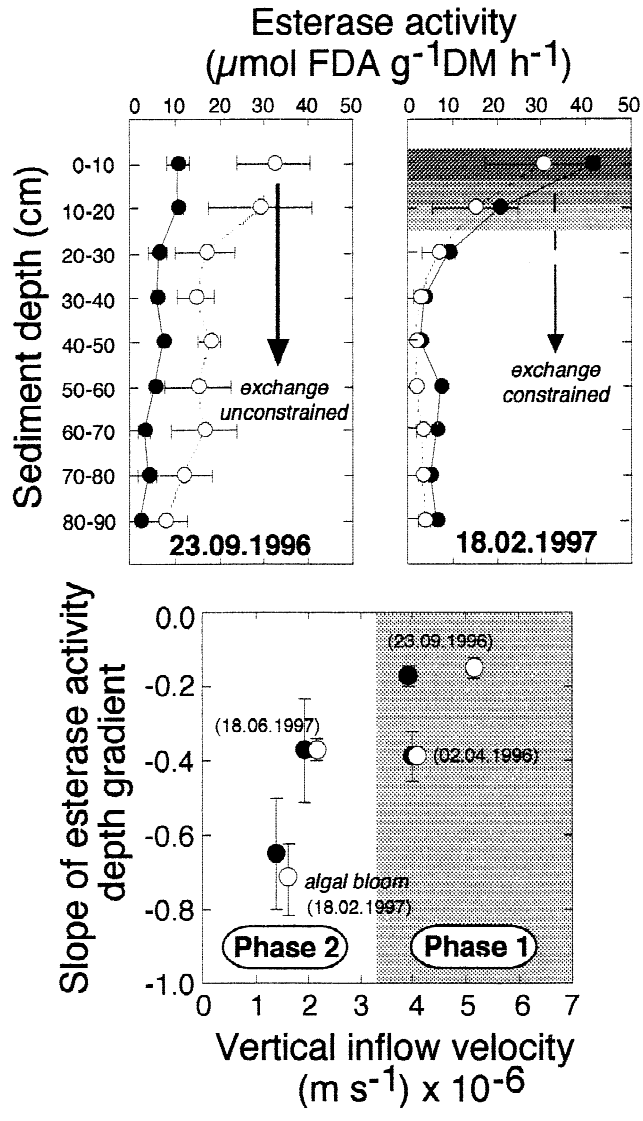

Fig. 6. Relationship between biofilm esterase activity and vertical inflow velocities. The upper panels show representative depth gradients of esterase activity (average ± S.E.) under hydrologically unconstrained (clogging phase 1) and constrained (clogging phase 2) conditions. The lower panel relates esterase activity gradients to vertical inflow velocities. The esterase gradient corresponds to the slope of the exponential model $y = e(k + c^*x)$, where y equals the esterase activity (µmol FDA h^{-1} g^{-1} DM) and x refers to the sediment depth (cm). Open dots designate SSF samples; closed dots designate OBB samples.

creased microbial biomass. However, the relationships are complex, and considerable disparities between experiments result from the granulometry of substrate, bacterial strains employed, and the techniques used to estimate their biomass. For instance, Taylor and Jaffé [38] found hydraulic conductivity decreasing exponentially with organic C $\leq$ 0.4 mg cm^{-3}, yet no relationship for organic C concentrations $\geq$0.4 mg cm^{-3}. Conversely, Vandevivere and Baveye [42] found no reduction of the hydraulic conductivity for biomass densities <4 mg wet weight cm^{-3}, yet significant reduction above that threshold concentration.

The significant temporal increase of the OBB esterase activity that is gradually transmitted towards depth (down to 50 cm, Fig. 4) suggests organic substrates (e.g., containing ester bonds) being rapidly entrained from the surface water by inflow fluxes and gradually immobilized and hydrolyzed by biofilms along their passage through the sediment. Therefore, the most active zone is restricted to the water/sediment interface, which agrees with observations from the Rhône River [28]. Furthermore, the predominantly horizontal water flow in deeper sediment layers (Fig. 2) is assumed to accentuate this pattern. The highly active interfacial sediments sequester nutrients and matter, and deeper interstitial water thus becomes a poor source to biofilms. Also, gradients of esterase activity became more apparent with ongoing clogging (Fig. 4). This prompted us to hypothesize that on-

Table 3. Pearson's correlation coefficient between C-carbohydrates and uronic acids and sediment bacterial abundance, chlorophyll *a*, pheophytin for three pooled depths layers in the Danube channel sites SSF and OBB

		C-Carbohydrates			Uronic acids		
Depth	Independent variable	Pearson's *r*	*p*	*n*	Pearson's *r*	*p*	*n*
Site SSF							
0–20 cm	Bacteria	0.112	0.715	18	0.172	0.573	18
	Chlorophyll*a*	0.723	0.003	20	0.689	0.004	20
	Pheophytin	0.783	0.001	20	0.735	0.003	20
20–40 cm	Bacteria	0.732	0.009	14	0.693	0.004	14
	Chlorophyll*a*	0.759	0.018	14	0.756	0.018	14
	Pheophytin	0.828	0.006	14	0.889	0.001	14
40–90 cm	Bacteria	nd[a]	nd	nd	nd	nd	nd
	Chlorophyll*a*	0.073	0.732	12	0.213	0.507	12
	Pheophytin	0.032	0.824	12	0.090	0.792	12
Site OBB							
0–20 cm	Bacteria	−0.418	0.201	11	−0.392	0.232	11
	Chlorophyll*a*	0.695	0.014	12	0.472	0.121	12
	Pheophytin	0.595	0.041	12	0.373	0.232	12
20–40 cm	Bacteria	−0.185	0.525	14	−0.169	0.562	14
	Chlorophyll*a*	0.121	0.795	7	−0.118	0.801	7
	Pheophytin	0.357	0.255	12	0.198	0.538	12
40–90 cm	Bacteria	nd	nd	nd	nd	nd	nd
	Chlorophyll*a*	−0.469	0.202	9	−0.432	0.245	9
	Pheophytin	−0.493	0.087	13	−0.373	0.209	13

[a] not determined.

going clogging reduces the mass transfer from the surface water into the river bed. As a consequence, biofilm esterase activity was expected to exhibit increasingly higher gradients toward depth. We found, in fact, the lowest slope of the exponential model that relates esterase activity to sediment depth concurring with high inflow velocities during the first clogging phase (Fig. 6), whereas the highest slope that translates into a relatively steep hydrolytic depth gradient coincided with the algal bloom during the second clogging phase. This strongly points to an important role for algae in the clogging process.

Low winter discharge (see Fig. 1) along with low turbidity caused a benthic algal bloom in February 1997. Substantial amounts of predominantly filamentous algae were reported by scuba divers and confirmed by video imagery that covered large areas of the river bed. The relationships we detected between chlorophyll *a*, pheophytin, and C–CHO, UAc (see Table 4) suggest considerable algal participation in the carbohydrate pool and agrees with studies from marine sediments [40]. Decaying algal cells can, for instance, di-

Table 4. Multiple regression of biofilm esterase activity in relation to chlorophyll *a*, C-carbohydrate concentration and bacterial abundance in OBB and SSF

Site SSF			
Term entered	Partial *r*	*p*	Model r^2
Chlorophyll *a*	0.501	0.007	0.251
Bacteria	−0.498	0.008	0.437
C-Carbohydrates	−0.386	0.051	0.521
Multiple r^2	*F*-ratio	*P*	*N*
0.521	8.695	0.0004	28
Site OBB			
Term entered	Partial *r*	*p*	Model r^2
Chlorophyll *a*	0.791	0.001	0.640
C-Carbohydrates	−0.634	0.027	0.784
Multiple r^2	*F*-ratio	*P*	*N*
0.784	18.021	0.0005	13

Table 5. Grain size analysis of sediment used in assays. Sediment samples bulked over depth and time[a]

Site[b]	D_{10}	D_{25}	D_{50}	D_{75}
SSF	109.1	194.0	264.4	359.0
OBB	103.8	182.9	271.8	379.5

[a] Subscript numbers denote quantiles (μm).
[b] Wilcoxon signed ranks test, $Z = 0.365$, two-sided $p = 0.71$.

rectly contribute to the carbohydrate pool via cell leakage or release of molecules normally bound to the living cell [40]. Complementarily, the algal exudates of senescing cells can serve as growth substrate for heterotrophic biofilm bacteria (e.g., [22]), which in turn produce exopolymers. We consider the relationship between bacterial abundance and esterase activity (Table 5) as further evidence toward algal/bacterial interactions in the Danube River bed. Certainly, algae also express esterases, but because of high bacterial biomass and metabolism the observed esterase activity can primarily be ascribed to bacteria. Bacteria accounted for the bulk of the biofilm associated C and their biomass gradually increased from ~87 to 94% in SSF and from ~69 to 95% in OBB biofilms from clogging phase 1 to 2. We are therefore inclined to relate clogging of the Danube River bed to the accumulation of bacterial cells—fostered by algae—rather than to their exopolymers. This agrees with Vandevivere and Baveye [42], who found bacterial cells responsible for the decline of the hydraulic conductivity in sand columns.

In conclusion, we were able to relate spatial and temporal patterns of sediment biofilm esterase activity and carbohydrate exopolymers to hydrodynamic constraints in a large and deep river. On the other hand, our data are the first to link natural microbial biofilms to river bottom clogging. However, evaluating the action of microbes on clogging under field conditions is not obvious because we were not able to unequivocally partition the effects of conservative solids and microbial cells and to recognize thereby functional relationships between biotic and physical processes. Experiments with sediment columns, natural microbial communities, and particle and nutrient inputs as they occur in the surface water are needed now to partition the multiple effects.

Acknowledgments

We acknowledge Iris Kremlicka, Ingrid Kolar, and Albert Brugger for their excellent laboratory work. Gerhard Herndl commented on an earlier version of the paper. Roland Schmalfuss generously made available groundwater flow velocity data. Financial support came from the Austrian Verbund Gesellschaft to Gerhard Herndl. TJB was partially supported by a grant from the Austrian Ministery of Sciences.

References

1. Battin TJ (1997) Assessment of fluorescein diacetate hydrolysis as a measure of total esterase activity in natural stream sediment biofilms. Sci Tot Environm 198:51–60
2. Buffle J, Leppard GG (1995) Characterization of aquatic colloids and macromolecules. 1. Structure and behavior of colloidal material. Environm Sci Technol 29:2169–2175
3. Blenkinsopp SA, Lock MA (1994) The impact of storm-flow on river biofilm architecture. J Phycol 30:807–818
4. Carling PA (1992) In-stream hydraulics and sediment transport. In: Calow P, Petts GE (eds) The Rivers Handbook, Vol 1. Blackwell Scientific Publications, pp 101–125
5. Claret C, Fontvieille D (1997) Characteristics of biofilm assemblages in two contrasted hydrodynamic and trophic contexts. Microbiol Ecol 34:49–57
6. Cloern JE, Grenz C, Vidergar-Lucas L (1995) An empirical model of the phytoplankton chlorophyll:carbon ratio—the conversion factor between productivity and growth rate. Limnol Oceanogr 40:1313–1321
7. Corpe WA (1970) An acid polysaccharide produced by a primary film-forming marine bacterium. Develop Ind Microbiol 11:402–412
8. Cunningham AB, Characklis WG, Abedeen F, Crawford D (1991) Influence of biofilm accumulation on porous media hydrodynamics. Environm Sci Technol 25:1305–1311
9. De Beer D, Stoodley P, Roe F, Lewandowski Z (1994) Effects of biofilm structures on oxygen distribution and mass transport. Biotechnol Bioeng 43:1131–1138
10. Decho AW (1990) Microbial exopolymer secretions in ocean environments: their role(s) in food webs and marine processes. Oceanogr Mar Biol Annu Rev 28:73–153
11. Dubois M, Gilles KA, Hamilton JK, Rebers PA, Smith R (1956) Colorimetric method for the determination of sugars and related substances. Anal Chem 28:350–356
12. Elliott AH, Brooks NH (1997) Transfer of nonsorbing solutes to a streambed with bed forms: Theory. Wat Res Res 33:123–136
13. Farnleitner A, Kasimir DG (1996) Bacterial activities in newly deposited sediments of the river Danube. Arch Hydrobiol Suppl 113:397–403
14. Filisetti-Cozzi TMCC, Carpita NC (1991) Measurement of uronic acids without interference from neutral sugars. Anal Biochem 197:157–162
15. Fontvieille D, Outaguerouine A, Thevenot DR (1992) Fluorescein diacetate hydrolysis as a measure of microbial activity in aquatic systems: application to activated sludges. Environm Technol 13:531–540
16. Fowler J, Cohen L (1990) Practical statistics for field biology. Open University Press
17. Freeman C, Lock MA (1995) The biofilm polysaccharide matrix: A buffer against changing organic substrate supply? Limnol Oceanogr 40:273–278
18. Grant J, Gust C (1987) Prediction of coastal sediment stability from photopigment content of mats of purple sulphur bacteria. Nature 330:244–246
19. Hendricks SP (1992) Bacterial dynamics near the groundwater–surface water interface (hyporheic zone) beneath a sandy-bed, third order stream in northern Michigan. In: Stanford JA, Simons JJ (eds) Proceedings of the First International Con-

ference on Groundwater Ecology, American Water Resource Association, pp 27–35
20. Humpesch UH, Niederreiter R (1993) Freeze-core method for sampling the vertical distribution of the macrozoobenthos in the main channel of a large deep river, the River Danube at river kilometre 1889. Arch Hydrobiol Suppl 103:87–90
21. Kaplan D, Christiaen D, Arad SM (1987) Chelating properties of extracellular polysaccharides from Chlorella spp. Appl Environm Microbiol 53:2953–2956
22. Lawrence JR, Korber DR, Wolfaardt GM, Caldwell DE (1995) Behavioral strategies of surface-colonizing bacteria. Advances Microb Ecol 14:1–75
23. Lee S, Furhman JA (1987) Relationships between biovolume and biomass of naturally derived marine bacterioplankton. Appl Environm Microbiol 53:1298–1303
24. Leff LG (1994) Stream bacterial ecology: A neglected field. ASM News 60:135–138
25. Leichtfried M (1996) Organic matter in bed-sediments of the River Danube and a small unpolluted stream, the Oberer Seebach. Arch Hydrobiol Suppl 113, pp 1–4
26. Lock MA (1993) Attached microbial communities in rivers. In: Ford TE (ed) Aquatic microbiology. An ecological approach. Blackwell, pp 113–138
27. Lozada de DS, Vandevivere P, Baveye P, Zinder S (1994) Decrease of the hydraulic conductivity of sand columns by *Methanosarcina barkeri.* World J Microbiol Biotechnol 10: 325–333
28. Marmonier P, Fontvieille D, Gibert J, Vanek V (1995) Distribution of dissolved organic carbon and bacteria at the interface between the Rhône River and its alluvial aquifer. J N Am Benthol Soc 14:382–392
29. Morel-Seytoux HJ (1988) Soil–aquifer–stream interactions—a reductionist attempt toward physical–stochastic integration. J Hydrol 102:355–379
30. Neu TR, Lawrence JR (1997) Development and structure of microbial biofilms in river water studied by confocal laser scanning microscopy. FEMS Microbiol Ecol 24:11–25
31. Parsons T, Maita Y, Lalli C (1984) A Manual of Chemical and Biological Methods for Seawater Analysis. Pergamon Press
32. Porter KG, Feig YG (1980) The use of DAPI for identifying and counting aquatic microflora. Limnol Oceanogr 25:943–948
33. Sengschmitt D, Steiner KH, Blaschke AP, Schmalfuss R (1998) Einfluss der Kolmation auf den Grundwasserhaushalt am Beispiel des Stauraumes Freudenau. Wiener Mitteilunger, Wasser-Abwasser-Gewässesr 148:321–350
34. Shaw JC, Bramhill B, Wardlaw NC, Costerton JW (1985) Bacterial fouling in a model core system. Appl Environm Microbiol 49:693–701
35. Shepherd RG (1989) Correlations of permeability and grain size. Ground Water 27:633–638
36. Stoodley P, DeBeer D, Lewandowski Z (1994) Liquid flow in biofilm systems. Appl Environm Microbiol 60:2711–2716
37. Sutherland IW (1985) Biosynthesis and composition of gram-negative bacterial extracellular and wall polysaccharides. Ann Rev Microbiol 39:243–270
38. Taylor SW, Jaffé PR (1990) Biofilm growth and the related changes in the physical properties of a porous medium. 1. Experimental investigation. Wat Res Res 26:2153–2159
39. Uhlinger DJ, White DC (1983) Relationship between physiological status and formation of extracellular polysaccharide glycocalyx in *Pseudomonas atlantica.* Appl Environm Microbiol 45:67–70
40. Underwood GJC, Paterson DM, Parkes RJ (1995) The measurement of microbial carbohydrate exopolymers from intertidal sediments. Limnol Oceanogr 40:1243–1253
41. Vandevivere P, Baveye P (1992) Effect of bacterial extracellular polymer on the saturated hydraulic conductivity of sand columns. Appl Environm Microbiol 58:1960–1698
42. Vandevivere P, Baveye P (1992) Saturated hydraulic conductivity reduction caused by aerobic bacteria in sand columns. Soil Sci Soc Am J 56:1–13
43. Vandevivere P, Kirchman D (1993) Attachment stimulates exopolysaccharide synthesis by a bacterium. Appl Environ Microbiol 59:3280–3286
44. Velji MI, Albright LJ (1985) Microscopic enumeration of attached marine bacteria of seawater, marine sediment, fecal matter, and kelp blade samples following pyrophosphate and ultrasound treatments. Can J Microbiol 32:121–126
45. Webster JR, Meyer JL (1997) Stream organic matter budgets. J North Am Benthol Soc 16
46. Wilkinson L (1992) SYSTAT 5.2. for the Macintosh. SYSTAT Inc, Evanston IL, USA